



Adsorption characteristics of Copper (II) ion on Cu-doped ZnO nanomaterials based on green synthesis from *Piper Chaudocanm* L. leaves extract

Thi Thao Truong¹ · Trung Hieu Le¹ · Tien Duc Pham²

Received: 7 July 2022 / Revised: 15 September 2022 / Accepted: 20 September 2022 / Published online: 28 September 2022
© The Author(s), under exclusive licence to Springer-Verlag GmbH Germany, part of Springer Nature 2022

Abstract

In this study, Cu-doped ZnO nanomaterials were fabricated by the sol–gel method using the extract of *Piper chaudocanum* L. leaves and the mixture of Zn (II) and Cu (II) salts. The Cu-doped ZnO nanomaterials changed from the $Zn_{1-x}Cu_xO$ solid solution into the ZnO/CuO nanocomposites with increasing Cu content from 1 to 10%. The monodisperse particles agglomerate into a block; the pyramidal blocks tend to form a longer and narrower in width at high Cu content with increasing porosity and adsorption sites. The pH_{pzc} of ZSCu10 was about 8.8. The Cu (II) adsorption increased with increasing the Cu content while the optimum conditions were found to be pH 7; adsorption time 120 min and adsorption efficiency at 1.0 g/l ZSCu10 or 10 ppm Cu (II) reached about 99%. The adsorption isotherms were fitted well with the Langmuir model while adsorption kinetics followed pseudo-second-order.

Keywords Cu-doped ZnO · Green synthesis · Cu (II) adsorption · *Piper chaudocanum* L. extract

Introduction

Copper was the first metal to be widely used by humans. The normal range of copper level in the dietary for adults is 1 to 3 mg/day and 0.1–1 mg/day in drinking water, which is needed for several functions in the human body [1]. In nature, Copper is found in ore deposits around the world. Copper is used for many different applications essential to modern life, such as electricity, electronics, telecommunications, and a high-quality material for architecture, both exterior and interior, gas piping systems, plumbing, fire sprinklers, and more. Copper is the second most used non-ferrous metal in the industry [2]. But, copper is considered one of the earliest known toxic metals. The copper content

in the environment is increasing due to the amount emitted from natural, from various industries, and also from man-made sources [3], raising serious environmental pollution.

For the removal of copper (heavy metal in general) from aqueous solutions, numerous conventional methods have been used, including chemical precipitation, flocculation, membrane filtration, ion exchange, electrochemical treatment, photo-catalysis, or adsorption [4–6]. Among these methods, adsorption is employed as the main concern of scientific research due to its high removal efficiency, ease of operation, and cost effectiveness. Various material has been studied for the adsorption of Cu (II) from aqueous solutions, such as biochar [3, 5], modification of biochar [7], chitosan and modified chitosan [8, 9], Martil sand [10], iron oxide coated sand [11], iron oxide [12], iron-perlite composite [6], biochar–biopolymeric hybrid [13], ZnO [14–16], ZnO hybrid [17], leaf powder [18], For those materials, ZnO and modified ZnO have received a lot of attention. ZnO is regarded as an environment friendly and low-cost multifunctional material. ZnO is not really a new material, but it has attracted research interest in recent decades because of its excellent properties and application [15, 19, 20]. ZnO is one of the nanometer-sized particles with the most diverse structure among all known materials: zero-dimensional (0D), 1D, 2D, and 3D. Each of these nanostructures can

✉ Thi Thao Truong
thao.tt@tnus.edu.vn

✉ Tien Duc Pham
tienduchphn@gmail.com; tienducpham@hus.edu.vn

¹ Department of Chemistry, TNU-University of Sciences, Thai Nguyen 250000, Vietnam

² Faculty of Chemistry, University of Science, Vietnam National University, Hanoi, 19 Le, Thanh Tong, Hoan Kiem, Hanoi 100000, Vietnam

occur in many different morphologies: nanorods, nanofibres, nanowires, nanotubes, nanorings, ... in 1D structures; nanosheets, nanopellets, ... in 2D or flower, snowflakes, in 3D [16, 21]. ZnO particles can be synthesized with differing shape, size, and spatial structure depending on the synthesis methods, conditions, and precursors in the synthesis process. In general, the specific surface area and the number of active surface site facilitating absorption increase with the decrease of ZnO nanoparticles (NPs). Practical studies have also demonstrated that ZnO and modified ZnO materials are good adsorbents for different types of pollutants: heavy metal, drug, dye, ... [15, 17, 21–28]. ZnO and modified ZnO can be synthesized by many methods, such as co-precipitation, sol–gel, hydrothermal, mechanochemical processes, and vapor deposition. In which, the sol–gel method is chosen by many researchers. But this method also has to use many different chemicals such as potassium hydroxide [29], ammonium solution [30], tartaric acid [31], oxalic acid [32], methanol and acetyl acetone [33], diethanolamine [34], 2-methoxyethanol and mono ethanolamine [35], m-cresol [36], citric acid and ethylene glycol [37], polyvinylpyrrolidone [38], Green synthesis recently attracts much attention. This method uses biomaterials as one of the precursors of the synthesis process, such as bacteria, fungi, yeasts, algae, plants, agricultural waste, ... [39–41], or using potential adsorption of agricultural waste materials (natural substances, by-products, agro-industrial wastes, or lignocellulosic wastes) [42]. Plant extract is the first choice due to its popularity, diversity, ease of regeneration, and environmentally friendly [43–45]. To enhance the adsorption efficiency of metal ions, there had been some studies of doping ZnO by some metals as Ag [46], Ga [47], modified surface ZnO by hybrid membranes [48], But doping ZnO by Cu (green synthesis or traditional synthesis method) has not been announced yet. In this study, Cu-doped ZnO nanomaterial was green synthesized by sol–gel method with precursors are only zinc acetate dihydrate (and copper (II) nitrate trihydrate) and aqueous extract of *Piper chaudiocanum* L. leaves. *P. chaudiocanum* L. is a medicinal in traditional Vietnamese medicine, which grows a lot in the Vietnam and some other Asian countries. Prepared Cu-doped ZnO was characterized and evaluated the Cu (II) adsorption from aqueous solution.

Materials and methods

Materials

Zinc acetate dehydrate ($\text{Zn}(\text{CH}_3\text{COO})_2 \cdot 2\text{H}_2\text{O}$, > 98%), copper (II) nitrate trihydrate ($\text{Cu}(\text{NO}_3)_2 \cdot 3\text{H}_2\text{O}$, > 99.5%), hydrochloric acid (HCl, 37%), sodium hydroxide pellets (NaOH, > 99%), and the stock solution 1000 ppm of Cu (II) were purchased from Merck company (Germany). All the

chemicals were analytical grade and were used as received without further purification. All working solution was prepared with double distilled water.

Green synthesis and characterization of Cu-doped ZnO NPs

Piper chaudiocanum L. leaves were thoroughly washed, dried, and then grinded into powder. Ten grams of the powder was ultrasound extracted by 100 mL of distilled water at 60 °C for 1 h. The extract was cooled, filtered, centrifuged, and then stored at 4 °C for further experiments. Completely dissolve mixture of zinc acetate and copper (II) nitrate (molar ratio 99:1; 95:5 and 90:10 respectively) was completely dissolved in 30 mL of distilled water, and 15 mL of extract was added drop by drop into the mixture solution at 70 °C under vigorous stirring, then heated at 80–90 °C to form a gel (approximately for 3 h), which was subsequently kept in an oven at 105 °C to obtain xerogel. Then, the xerogel was grounded into powders and then calcined at 450 °C for 1 h to get materials and denoted ZSCu1, ZSCu5, and ZSCu10, respectively. The same procedure was performed with the reaction between a solution of zinc acetate and oxalic acid (instead of the extract) [32]; the obtained product is denoted by ZnO.

The sample was characterized by X-ray diffractometer (Max 18XCE, Japan) equipped with $\text{CuK}\alpha$ radiation ($\lambda = 0.15406$ nm), scanning rate of $0.02^\circ \text{ s}^{-1}$ and 2θ ranges from 20 to 65°. Elemental analysis of samples was measured using Energy-dispersive X-ray spectroscopy (JSM-7900F). SEM images were obtained by scanning electron microscope (Leo 1430VP) at an accelerating voltage of 200 kV. Surface areas and porosity analysis were also performed the Brunauer–Emmett–Teller (BET) model (TriStar 3000 V6.07) with nitrogen gas at 77 K.

Determining the point of zero charge (pH_{pzc}), the 0.1 M NaCl solutions were prepared with an initial pH (pH_i) ranging from 3 to 11, and pH adjustment was performed with 0.1 M HCl and 0.1 M NaOH solutions. Five milligrams of sample was added to 10 mL of the NaCl solution prepared above. The mixture was shaken well for 1 h and then allows to stand at room temperature for 48 h before being filtered and the pH measured again. The point zero charge was obtained from the plot of ΔpH (change in pH) vs. initial pH.

Adsorption experiments

The adsorption experiments were investigated under a varying pH (4, 5, 6, and 7), time (10, 30, 50, 90, 120, and 180 min), adsorbent dosage (0.2, 0.5, and 1.0 g/L), and initial Cu (II) concentration (10, 20, and 30 ppm). In each test, a fixed amount of samples was added to a 10 mL Cu (II) solution of known concentration and pH which was contained

in a 15-mL falcon tube, followed by shaking for a time. And then, the solutions were centrifuged for 10 min at 5000 rpm, and the supernatant solution was taken out to analyze the remaining concentrations of Cu (II) ions by flame atomic absorption spectrometry (F-AAS). The adsorption experiments were executed in triplicates to calculate the average results. The adsorption capacity (q , mg/g) and adsorption efficiency (H , %) were calculated according to the formula:

$$q = \frac{(C_o - C_e)V}{m} \quad (1)$$

$$H\% = \frac{(C_o - C_e)}{C_o} \times 100\% \quad (2)$$

where V (L) is the volume of the solution, m (g) is the mass of the adsorbent, and C_o and C_e (mg/L) are the initial concentration and the concentration at adsorption equilibrium of Cu (II) ions.

The experimental results obtained were analyzed by some adsorption isotherm, adsorption kinetic, and adsorption thermodynamic models.

Results and discussion

Characterization

Structural and elemental characterizations

The crystal structure and phase purity of as-prepared samples were explored by XRD and are presented in Fig. 1a. The XRD patterns of the ZSCu1 sample show clear characteristic diffraction peaks of ZnO material at 2θ around 31.7° , 34.4° , 36.2° , 47.5° , 56.6° , 62.8° , 67.9° , and 69.1° corresponding to the Miller plane (1 0 0), (0 0 2), (1 0 1), (1 0 2), (1 1 0), (1 0 3), (1 1 2), and (2 0 1) respectively

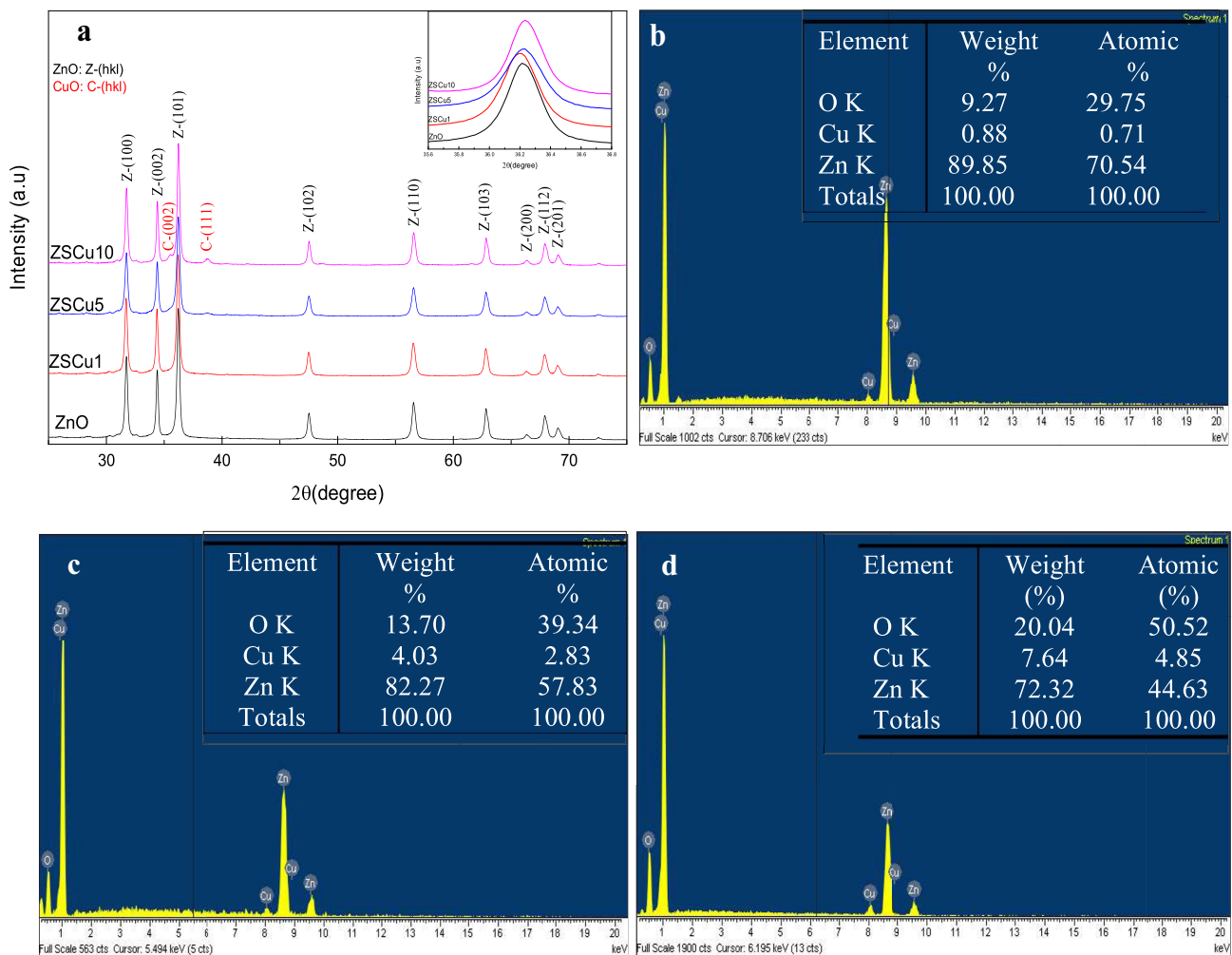


Fig. 1 XRD patterns of synthesized samples **(a)** and EDX spectra of ZSCu1 **(b)**, ZSCu5 **(c)**, and ZSCu10 **(d)**

(JCPDS card no. 00–036–1451) [49]. Thus, the crystal structure of the ZSCu1 sample belongs to the hexagonal wurtzite structure. There are no peaks concerning to the impurity phase. It is observed that the diffraction peak positions of the ZSCu1 sample shift slightly toward a low angle, as seen in the inset of Fig. 1. The shifting of diffraction pattern observed in the ZSCu1 sample approves for the modification of the crystal structure of ZnO, meaning the formation of $Zn_{1-x}Cu_xO$ solid solution for the ZSCu1 sample. The other samples show a complete coincidence of the Bragg peak positions of ZnO and ZSCu5 and ZSCu10 samples, but a change in the intensity of the diffraction profiles (0 0 2) and (1 1 1) is clearly observed. It means that the prepared ZSCu5 and ZSCu10 are formed into the ZnO/CuO nanocomposites instead of the $Zn_{1-x}Cu_xO$ solid solution [50]. The particle size is calculated by using the Debye–Scherrer equation; the values are about 34, 32, 27, and 29 nm for ZnO, ZSCu1, ZSCu5, and ZSCu10, respectively.

The element molar ratios in prepared samples are calculated based on the EDX spectra (Fig. 1b, c, d). Within the detection limit of the device, only characteristic peaks of Zn, Cu, and O appear; no other peaks of other elements can be detected. The Zn/Cu ratio from the EDX spectrum is about 70.04/0.71, 57.83/2.83, and 44.63/4.85 corresponding to the Cu content in the sample ZSCu1, ZSCu5, and ZSCu10 is 1.00%, 4.67%, and 9.80%, respectively. This experimental Cu content is equivalent to the design value.

Surface characterizations

The morphology and the surface feature of prepared samples are assessed by SEM (Fig. 2), BET (Fig. 3a), and pH_{pzc} (Fig. 3b). The ZnO nanoparticles are monodisperse, fairly homogeneous, and rather loosely bound (Fig. 2a). But, in the Cu-doped ZnO materials (Fig. 2b, c, d), the particles are

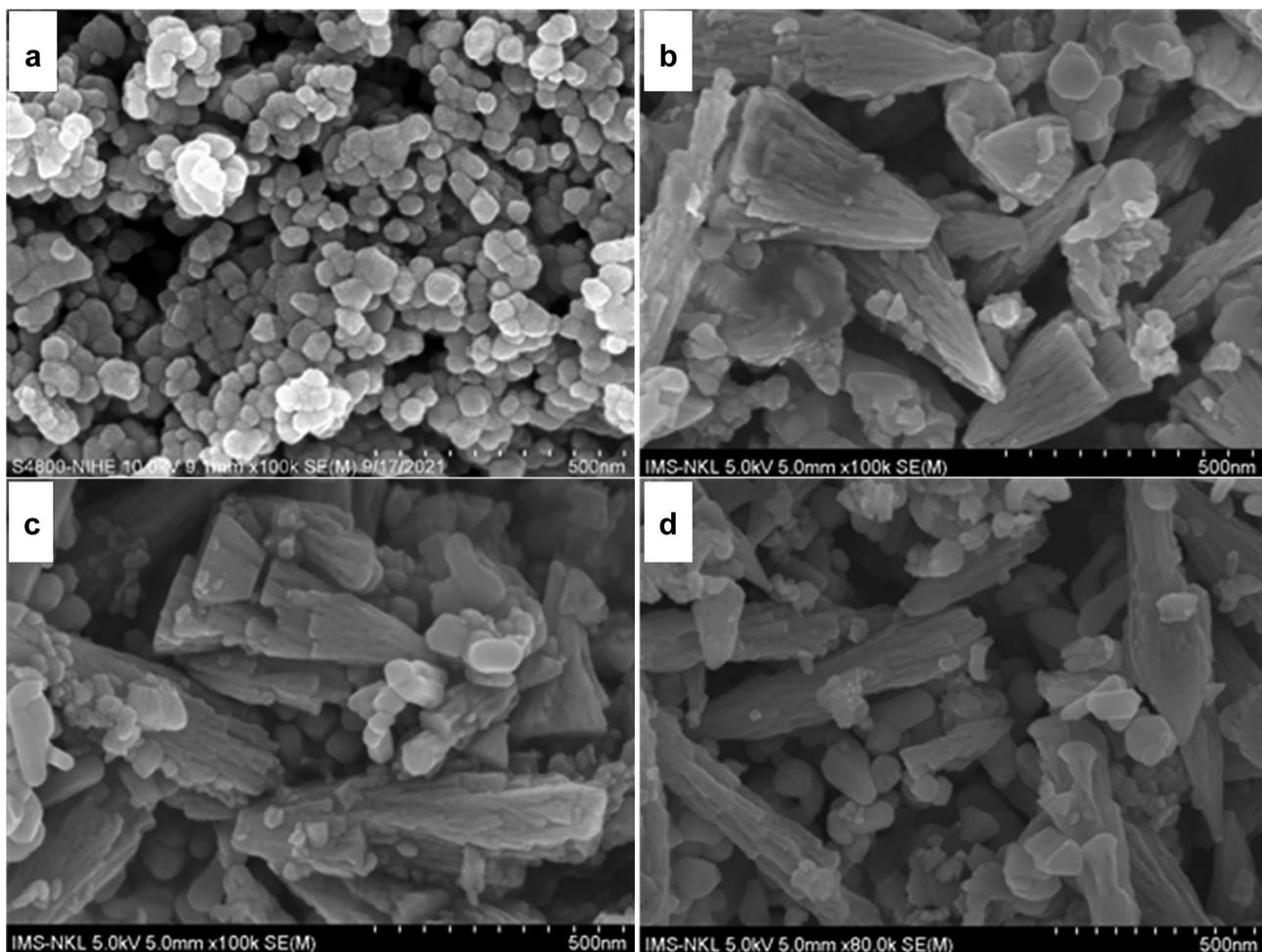


Fig. 2 SEM image of prepared materials: (a) ZnO, (b) ZSCu1, (c) ZSCu5, (d) ZSCu10

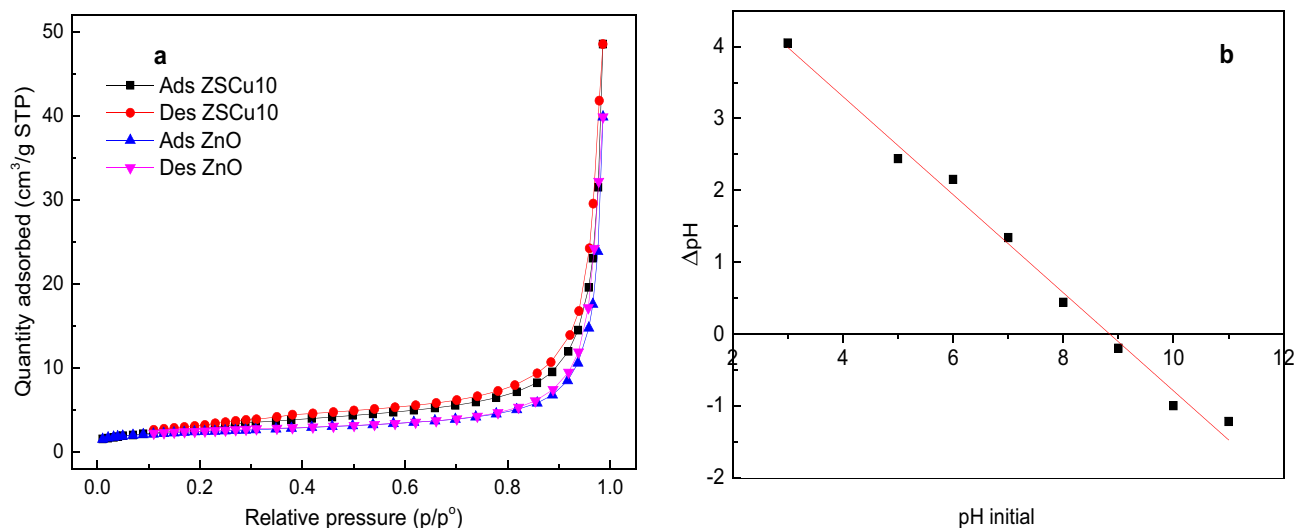


Fig. 3 (a) Nitrogen adsorption isotherm of ZnO and ZSCu10 and (b) the change of pH for determining the pH_{pzc} of ZSCu10

bigger size and agglomerated into a block, including pyramidal and smaller blocks that undefined shape. The higher the Cu content, the pyramidal blocks tend to be longer and narrower in width. This agglomeration can increase the porosity of the system, which also becomes available adsorption sites and enhances the available adsorption capacity. The morphology analysis is consistent with the results obtained from the BET analyses [51] and the following adsorption experimental results.

Figure 3a shows the N_2 adsorption/desorption isotherms for the prepared ZnO and ZSCu10; the isotherm linear plots were of type V, which indicated the ZnO and ZSCu10 particles are both meso-porous a structure [52]. The BET surface area (m^2/g), pore volumes (cm^3/g), and pore diameter (nm) are found to be about 8.58, 0.048, and 28.90 for ZnO and 11.05, 0.057, and 33.74 for ZSCu10. The doping of ZnO by Cu leads to the change in the structure of ZnO [53], and the *P. chaudiocanum* L. leaves extract with complex organic ingredients (phenolic, flavonoid groups, ...) not only acted as a complexing agent with metal ions but also acted as a surfactant. These mechanisms had contributed to the reduced agglomeration of initial ZnO blocks, making them more porous, and specific surface area increased [54].

The pH_{pzc} is an important characteristic of adsorbents. Figure 3b shows that the point zero charge of ZSCu10 is 8.8. It means that the surface charge of ZSCu10 is positive and vice versa at a solution pH less than 8.8. As pH increases, the surface positive charge is decreased, while the surface negative charge shows an opposite trend. This result is similar to ZnO which was synthesized by extract of *Saccharomyces cerevisiae* [40].

Adsorption studies

The effect of factors on adsorption is first studied as the solution pH: 5 mg ZSCu5 is added to 10 mL of 20 ppm Cu (II) solution pH from 3 to 7, shaken for 3 h at 22 °C. The experimental results are shown in Fig. 4a. As pH increases, the removal of Cu (II) from the solution is increased. This result is consistent with the results of determining the pH_{pzc} of the material: the surface charge of the adsorbent decreases gradually, changing from positive to negative as the pH increases, so that, at low pH, very few Cu (II) ions (positively charged) can be adsorbed because of electrostatic repulsion, and ZnO is partially dissolved. As the pH values increased, the electrostatic repulsion decreases, so the adsorption of Cu (II) ion into the adsorbent surface increases and reached maximum at pH 7.0. In this study, $pH > 7$ is not considered because of the formation of hydroxyl of the Cu (II). For this reason, the optimum pH is selected to be 7.0 for further experiments.

Next, the influence of doped Cu into ZnO materials and adsorption time is investigated: The adsorption experiment was conducted with 20 ppm Cu (II) solution, $pH = 7$, adsorbent dosage of 0.5 g/L at the time of 10, 30, 60, 90, 120, and 180 min at 22 °C. The experimental results are shown in Fig. 4b. In general, as adsorption time increases, the doped Cu content increases and Cu (II) adsorption increases: the time to reach adsorption equilibrium is about 120–180 min; after 3 h of adsorption, the Cu (II) ion removal from solution by 0.5 g/L ZnO, ZSCu1, ZSCu5, and ZSCu10 is 91.7% to 93.6%, 94.7%, and 95.8%, respectively. According to the XRD analysis results, the increase of Cu content leads to the

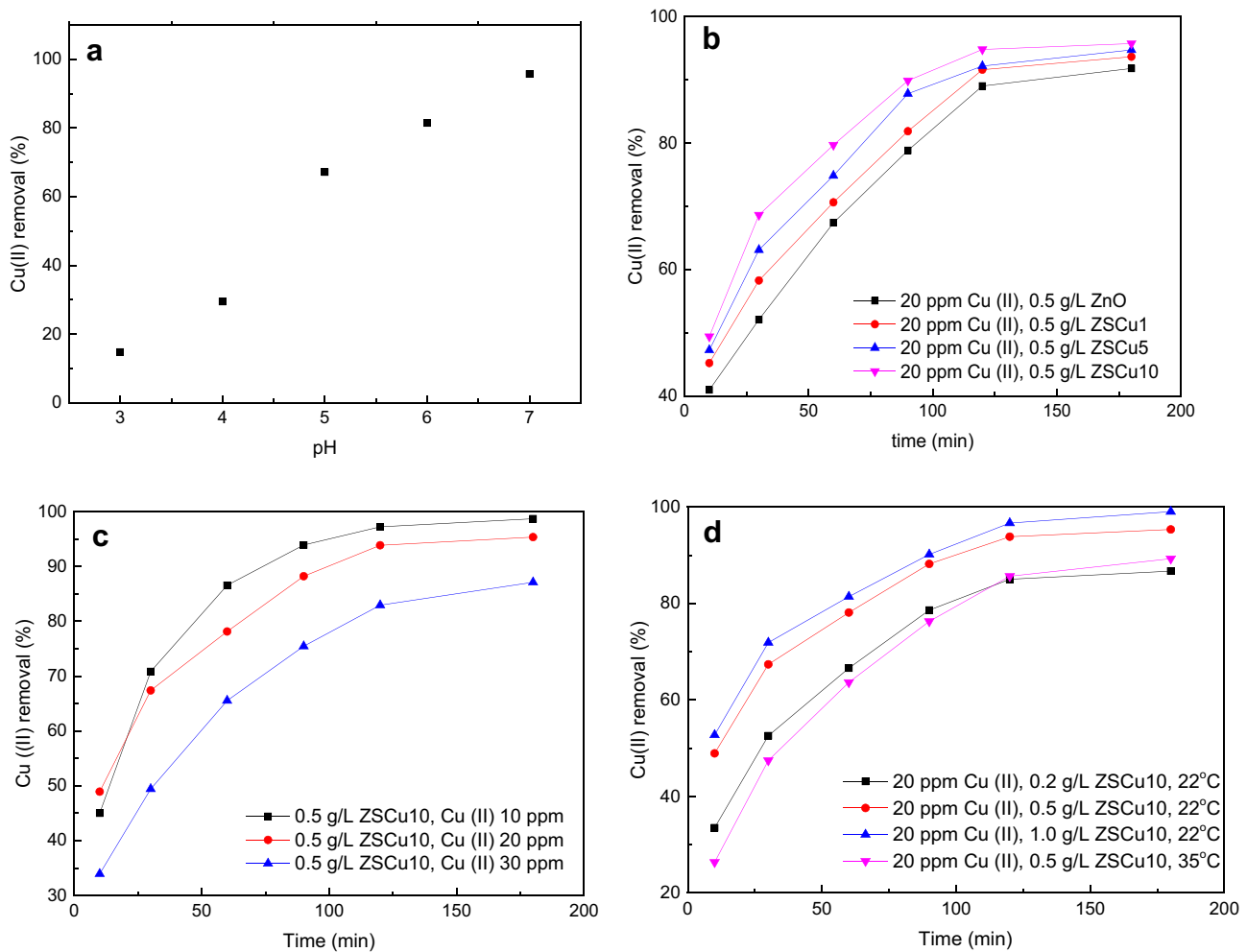


Fig. 4 Copper removal efficiency by pH (a), time and doped Cu content (b), time and initial Cu (II) concentration (c), and time, temperature, and adsorbent dosage (d)

formation of ZnO/CuO composite, so it enhances the formation of congruent ion pair $\text{Cu}^{2+}/\text{Cu}^{2+}$ between the adsorbent and adsorbate, thus increasing the adsorption. For this reason, the ZSCu10 was selected for further experiments: the influence of initial Cu (II) concentration (from 10 to 30 ppm) and the adsorbent dosage (from 0.2 to 1.0 g/L) to the adsorption at 22 °C. The experimental results are shown in Fig. 4c, d. Adsorption increases as adsorbent dosage increases and initial Cu (II) concentration decreases. At the higher adsorbent dose or smaller initial adsorbate concentration, the greater the number of sites available for adsorption, the more favorable the adsorption [27]; at 1.0 g/L ZSCu10 or 10 ppm Cu (II), the adsorption efficiency reached about 99%. The effect of temperature to the adsorption was tested by the adsorption 20 ppm Cu (II) by 0.5 g/L ZSCu10 at 35 °C (Fig. 4d). As a result, as the temperature increased, the adsorption efficiency decreased. This result shows that the nature of the process is physical adsorption. Those

results are used for research adsorption isotherm, adsorption kinetic, and adsorption thermodynamic.

The morphology of ZSCu10 after Cu (II) ion adsorption is shown in Fig. 5. After the adsorption process at a temperature of 22 °C (Fig. 5a), it is easy to see that the grain boundaries between the particles in the block have been blurred, the surface of the blocks seems to have a fuzzy coating, and the image is not as sharp as the image before adsorption (Fig. 2d). With the ZSCu10 samples adsorbed at 35 °C (Fig. 5b), the original structural blocks are clearly broken. It due to the simultaneous effects of adsorption, temperature, and thermal motion between particles in the system. This also shows that the bond between ZnO/CuO nanocomposites particles is less stable, easily broken, and the aggregate particles are porous, better adsorbents than monodisperse.

The FTIR spectra of ZSCu10 NPs before and after adsorption Cu (II) from the water solution are shown in Fig. 6. All of them consist of a clearly peak in the region of

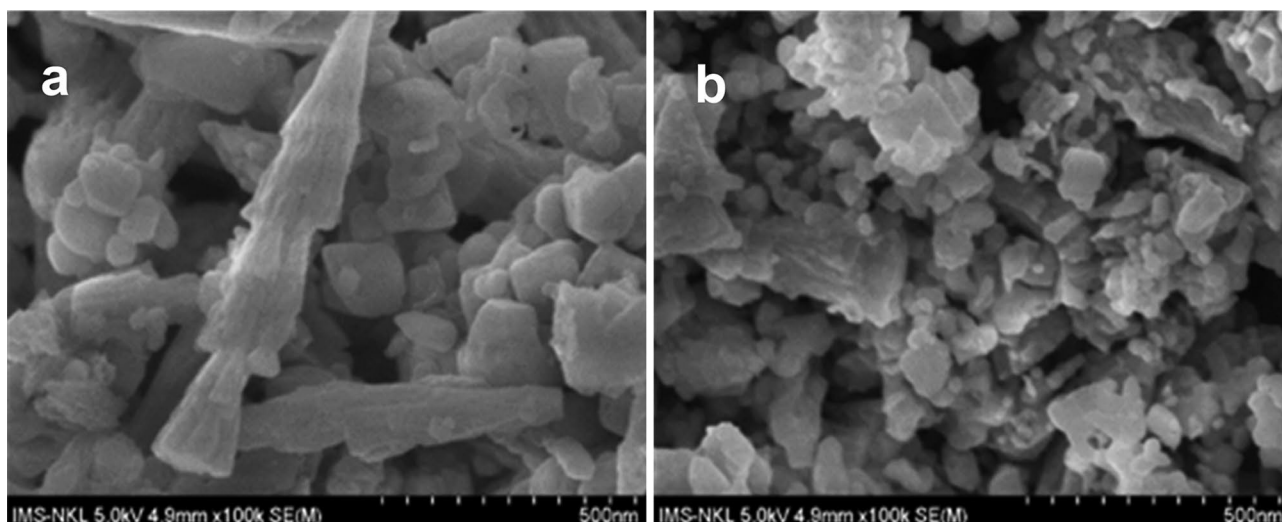
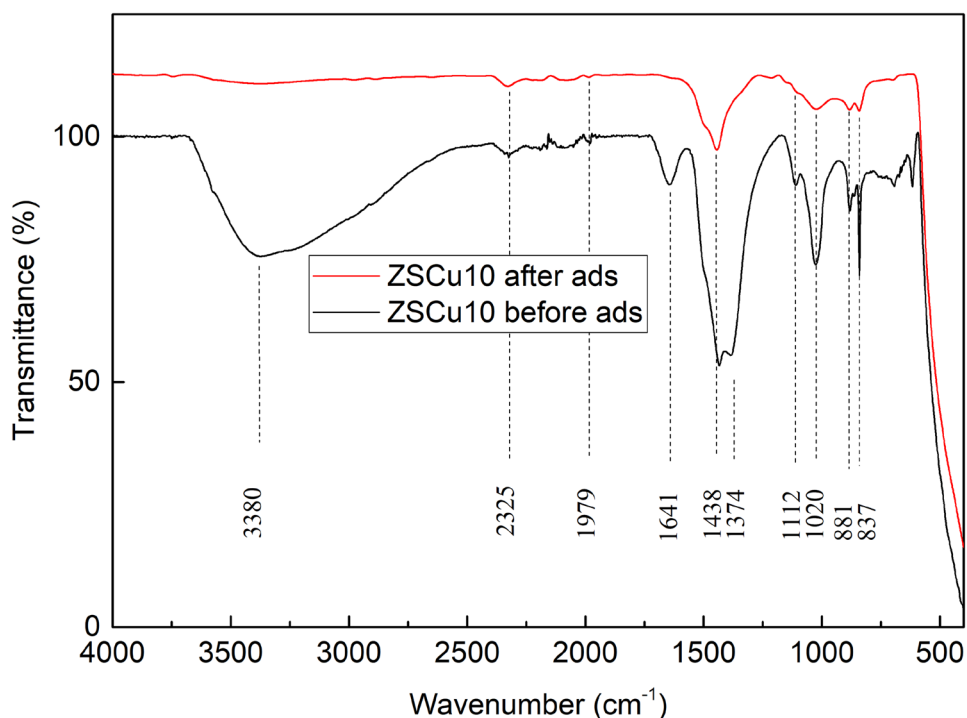


Fig. 5 SEM image of ZSCu10 after the adsorption process at 22 °C (a) and 35 °C (b)

under 500 cm^{-1} is assigned the stretching vibration of metal-O (Zn–O and Cu–O) bond. The FTIR spectra of ZSCu10 before the adsorption reveal the presence of –OH stretching vibrations at broad peaks around 3380 cm^{-1} , some shoulder peaks near 2300 cm^{-1} assigned to the C–N stretching vibration [55], and a peak at 1641 cm^{-1} is assigned the stretching vibrations of C=O bond; the peaks at 1438 cm^{-1} can be attributed to C–C in aromatic ring [56] or the C–H bending vibrations of aldehyde or ketonic functionality [57]; the peak at 1374 cm^{-1} and 1020 cm^{-1} is assigned the symmetric stretching of carboxylate and the stretching vibrations of

–C–O bond in the phenolic groups or carboxylic groups [58]; and other peaks at 1112, 881, and 837 cm^{-1} are assigned to various aromatic functionalities [57] or the Zn–OH peaks at 881 and 837 cm^{-1} . This is due to the oxidation of reactive carbonaceous material during calcinations and the adsorption of water over the surface of the calcined ZnO NPs. But, after the adsorption Cu (II) from the water solution, some peaks disappeared as at 3380, 1641, and 1374 cm^{-1} , or peak intensity decreased markedly as at 1438, 1112, 1020, 881, and 837 cm^{-1} are all characteristic for O–H, –C–O, –C=O or aromatic functional. It indicated that the formation the bond

Fig. 6 FTIR spectrum of ZSCu10 NPs before and after adsorption Cu (II)



of O-Cu²⁺ or/and Cu²⁺ with aromatic ring. From the result of adsorption decreased as temperature increased, it shows that the type of this bond can be electrostatic attraction between electron-rich agent and positive Cu²⁺ ion, a physical bond, not the chemical bond that is covalent bond type of electron donor–acceptor between the electron-paired pair of the electron-rich agent with an empty orbital of Cu²⁺ ion.

Adsorption isotherm

The experimental data were fitted using Langmuir, Freundlich, and Temkin isotherm according to the Eqs. (3), (4), and (5) and are listed below [59]:

$$\frac{C_e}{q_e} = \frac{1}{K_L \cdot q_{\max}} + \frac{C_e}{q_{\max}} \quad (3)$$

$$\text{Lg}(q_e) = \text{lg}(K_F) + \frac{1}{n} \text{lg}(C_e) \quad (4)$$

$$q_e = B \text{lg} K_T + B \text{lg} C_e \quad (5)$$

where K_L (L/mg), K_F (L/mg) and K_T (L/mg) are the adsorption constant for Langmuir, Freundlich, and Temkin isotherm model, respectively, $1/n$ implies the degree of non-linearity between solution concentration and adsorption in Freundlich equation, and B_1 is related to the heat of adsorption in Temkin equation. The linear fitting of adsorption isotherm models and the regression coefficient (R^2) value are presented in Fig. 7. If $R^2 \gg 1$ or $R^2 < 0$, the adsorption is undesirable or irreversible, and the common adsorption state is R^2 is between 0 and 1. The agreement between theory and experiment is obtained when R^2 approaches 1. In general, the correlation of Langmuir isotherm is higher than Freundlich and Temkin isotherm, with indicated that the Cu (II) ion adsorption is desirable and well matched with Langmuir model. This result suggests a monolayer adsorption of Cu (II) ion on the homogeneous surface of ZSCu10 [39]. As the initial Cu (II) concentration increases, the adsorbent dosage decreases, the coefficient decreases. It means that, the

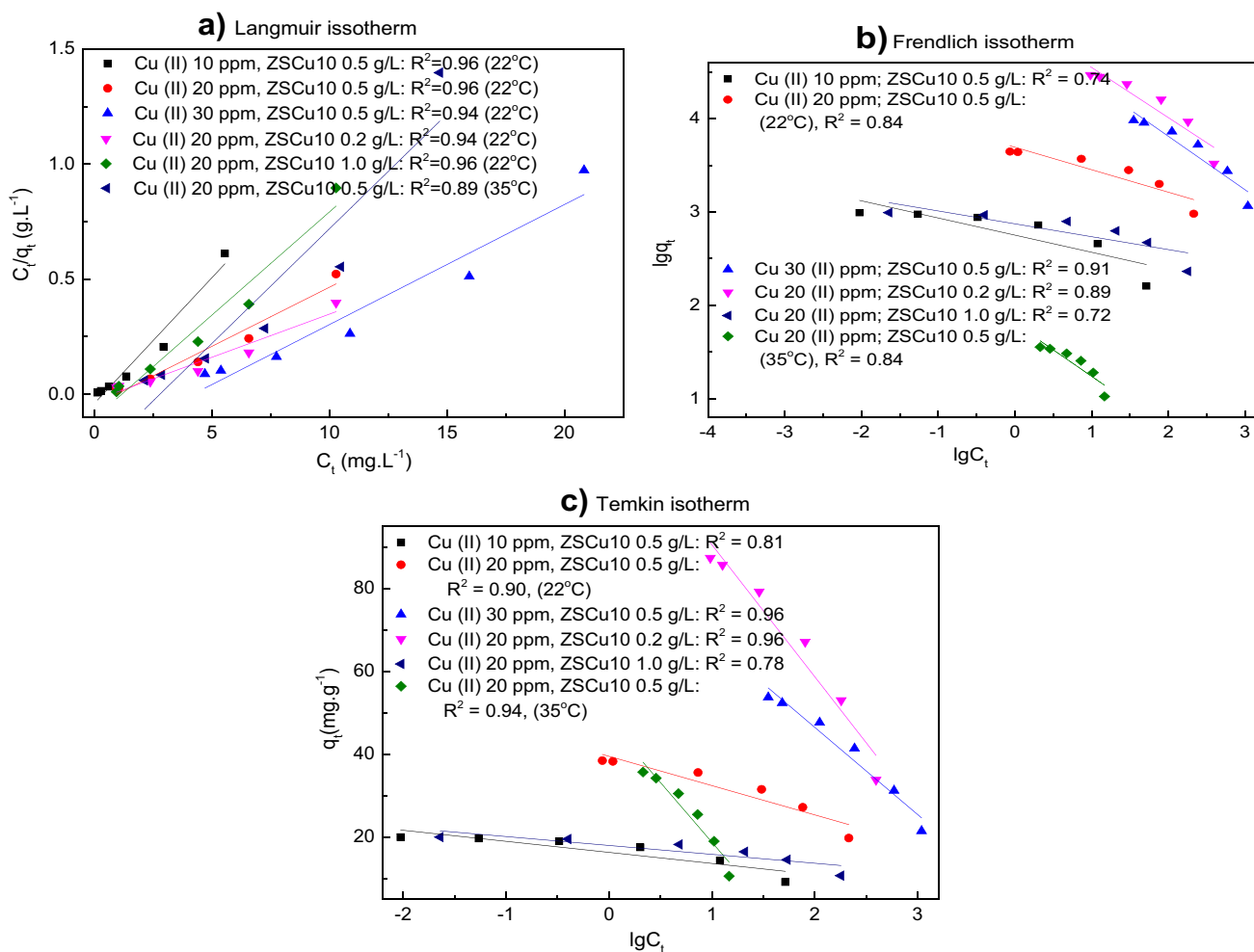


Fig. 7 Fitting of Langmuir (a), Freundlich (b), and Temkin (c) models to Cu(II) adsorption data

smaller the adsorbate concentration, the larger the adsorbent surface area, the more favorable the monolayer adsorption. Similar results were also obtained from Cu (II) ion adsorption studies [5, 7, 8].

However, there are some special cases: as the initial Cu (II) concentration increases (to 30 ppm), the adsorbent dosage decreases (to 0.2 g/L), and the temperature increases (to 35 °C), experimental data is more consistent with Temkin model than that with the Langmuir model ($R^2_{\text{Temkin}} > R^2_{\text{Langmuir}}$). When the initial Cu (II) concentration increases and the adsorbent dosage decreases, the monolayer adsorption according to the Langmuir model occurs as competitive adsorption, which according to the Temkin model, adsorption characteristic being a uniform distribution of binding energies, up to a maximum binding energy [60], the surface coverage of the adsorbent increases with a decrease in the heat of adsorption.

Adsorption kinetic

The experimental data were fitted using pseudo-first-order, pseudo-second-order, and intra-particle diffusion models according to the Eqs. (6), (7), and (8) and are listed below [18]:

$$\lg(q_e - q_t) = \lg q_e - k_1 t \quad (6)$$

$$\frac{t}{q_t} = \frac{1}{k_2 q_e^2} + \frac{t}{q_e} \quad (7)$$

$$q_t = k_{\text{id}} t^{0.5} + c \quad (8)$$

where k_1 (g/mg min), k_2 (g/mg min), and k_{id} (mg/g min^{0.5}) are the rate constants of the pseudo-first-order, pseudo-second-order, and intra-particle diffusion models, respectively; c

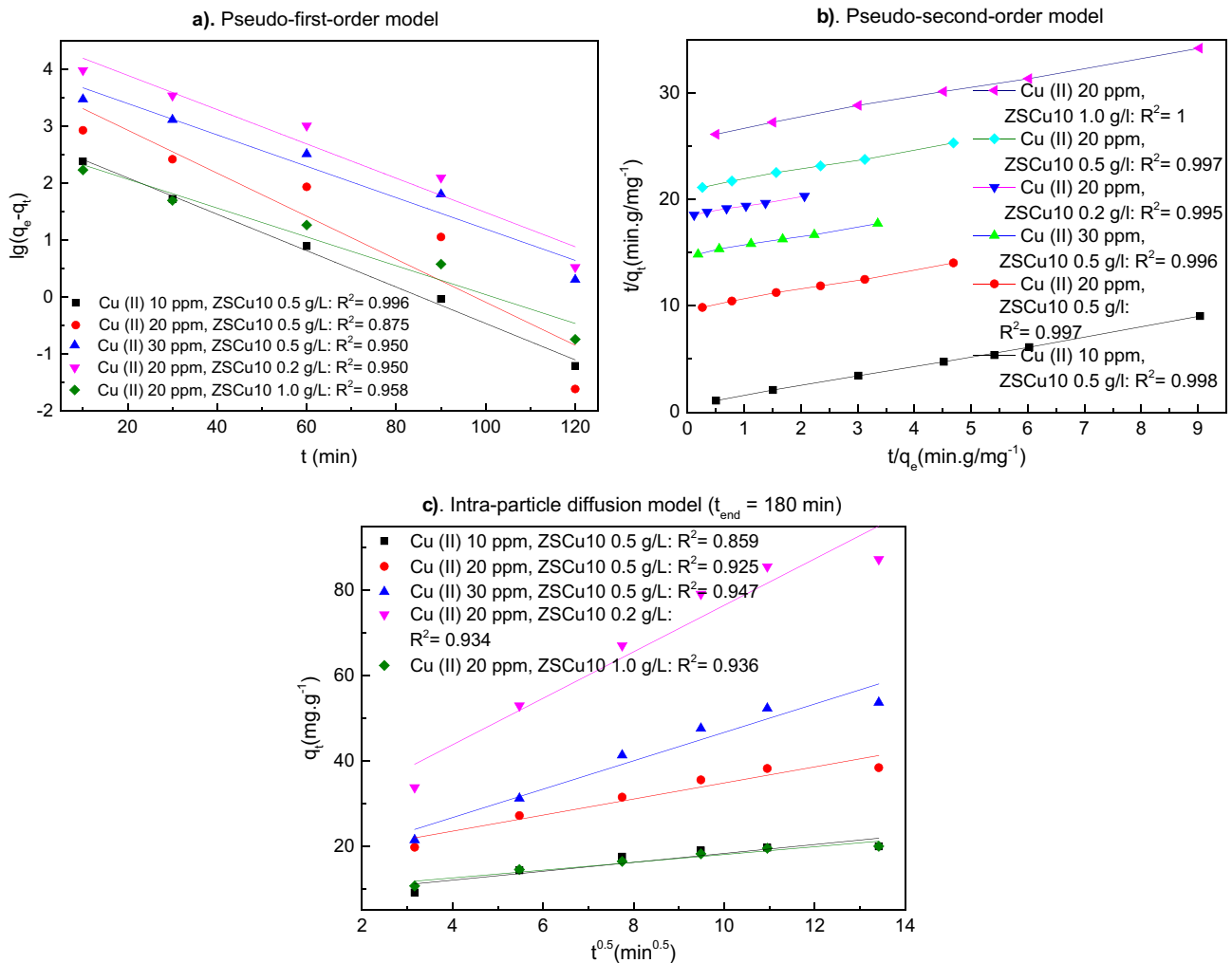


Fig. 8 Kinetic models for the adsorption of Cu (II) ions on ZSCu10 surface at pH 7

(mg/g) is the intercept of the intra-particle diffusion model, $q_e = q_{180}$.

The linear fitting of adsorption kinetic models, the equations, and the regression coefficient (R^2) value are presented in Fig. 8. According to obtained results, although the R^2 of the pseudo-first-order model and intra-particle diffusion model ($t_{\text{end}} = 180$ min) are all quite high, 0.859 to 0.996, the coefficient of pseudo-second-order model is highest. The sorption phenomenon of Cu (II) by ZSCu10 adsorbent follows the pseudo-second-order kinetics. The fitting is consistent with experimental results that both adsorbate and adsorbent concentrations are involved in the rate-limiting step. It means that the adsorption may include chemisorption, between the Cu (II) ions and ZSCu10 has occurred sharing or exchange of electrons, forming valence forces [61].

Adsorption thermodynamic

The adsorption equilibrium constant K_c , the enthalpy (ΔH), entropy (ΔS), and the Gibbs free energy of adsorption (ΔG) can be determined by the following equations [17]:

$$K_c = \frac{C_{\text{ads,e}}}{C_e} \quad (9)$$

$$\ln \frac{K_{T2}}{K_{T1}} = \frac{\Delta H}{R} \left(\frac{1}{T_1} - \frac{1}{T_2} \right) \quad (10)$$

$$\Delta G = -RT \ln K_c = \Delta H = T \Delta S \quad (11)$$

where $C_{\text{ads,e}}$ (mg/L) is the Cu (II) ion concentration on the adsorbent at equilibrium ($C_{\text{ads,e}} = C_0 - C_e$), R (8314 J/mol K) is the universal gas constant, T (Kelvin) is the absolute temperature.

The results obtained $K_{C,295} = 20.467$, $K_{C,308} = 8.333$, $\Delta H = -3.97$ kJ/mol, $\Delta G_{295} = -7.404$ kJ/mol, and $\Delta G_{308} = -5429$ kJ/mol indicate the spontaneous nature the adsorption of Cu (II) onto the ZSCu10 surface ($\Delta G < 0$), and the adsorption is more favorable at lower temperatures. The negative value of ΔH and the positive value of ΔS reveal that the Cu (II) adsorption onto the ZSCu10 is an exothermic process and takes place randomness at the solid-solution interface. The adsorption is dominated by physical adsorption.

Conclusions

The Cu-doped ZnO was synthesized by sol-gel method using *P. chaudocanum* L. leaves extract as a green precursor to replace conventional precursors. It slightly reduced the

particle size (from 34 nm of ZnO down to 27 nm ZSCu5) and increased the BET surface area (from 8.58 m²/g of ZnO to 11.05 m²/g of ZSCu10). They led to the adsorption efficiency of 20 ppm Cu (II) ion onto the surface of 0.5 g/L adsorbent at 22 °C increased from 91.7% (ZnO) to 95.8% (ZSCu10). The adsorption of Cu (II) onto ZSCu10 surface was investigated in detail; the influencing factors were as follows: pH of solution (4 to 7), initial concentration of Cu (II) ion (10 to 30 ppm), and adsorbent dosage (0.2 to 1.0 g/L), with different temperature values. The Cu (II) ions adsorption efficiency increased as the dose of adsorbent increases and the initial concentration of adsorbate decreases, at 1.0 g/L ZSCu10 or 10 ppm Cu (II) reached about 99%. Adsorption process was physical adsorption, spontaneous, and exothermic, followed by the Langmuir isotherm model and pseudo-second-order kinetic model.

Author contribution Thi Thao Truong: investigation, material synthesis, analyze, data treatment, writing, reviewing, editing, and supervision. Trung Hieu Le: methodology, analyze, and data treatment. Tien Duc Pham: conceptualization, writing, reviewing, and editing. All authors read and approved the final manuscript.

Declarations

Competing interests The authors declare no competing interests.

References

- Herschy RW (2012) Water quality for drinking: WHO guidelines. *Encycl Earth Sci Ser* 876–883. https://doi.org/10.1007/978-1-4020-4410-6_184
- Izydoreczyk G, Mikula K, Skrzypczak D, Moustakas K (2021) Potential environmental pollution from copper metallurgy and methods of management. *Environ Res* 197(March):111050. <https://doi.org/10.1016/j.envres.2021.111050>
- Bashir M, Tyagi S, Annachhatre AP (2020) Materials today : proceedings adsorption of copper from aqueous solution onto agricultural adsorbents : kinetics and isotherm studies. *Mater Today Proc* no. xxxx. <https://doi.org/10.1016/j.matpr.2020.05.287>
- Afroze S, Sen TK (2018) A review on heavy metal ions and dye adsorption from water by agricultural solid waste adsorbents. *Water Air Soil Pollut* 29(7). <https://doi.org/10.1007/s11270-018-3869-z>
- Katiyar R, Kumar A, Nguyen T, Rani R, Chen C, Dong C (2021) Bioresource technology adsorption of copper (II) in aqueous solution using biochars derived from *Ascophyllum nodosum* seaweed. *Bioresour Technol* 328(January):124829. <https://doi.org/10.1016/j.biortech.2021.124829>
- Shadi M, Mohamed Y, Ibrahim E, Garforth A, Alfutimie A (2020) Journal of water process engineering on copper removal from aquatic media using simultaneous and sequential iron-perlite composites. *J Water Process Eng* (November):101842. <https://doi.org/10.1016/j.jwpe.2020.101842>
- Liu J, Cheng W, Yang X, Bao Y (2019) Modification of biochar with silicon by one-step sintering and understanding of adsorption

- mechanism on copper ions. *Sci Total Environ* 135252. <https://doi.org/10.1016/j.scitotenv.2019.135252>
8. Ahmad M et al (2019) New method for hydrogel synthesis from diphenylcarbazide chitosan for selective copper removal. *Int J Biol Macromol* 136:189–198. <https://doi.org/10.1016/j.ijbiomac.2019.06.084>
 9. Rakati KK, Mirzaei M, Maghsoodi S, Shahbazi A (2019) International Journal of Biological Macromolecules Preparation and characterization of poly aniline modified chitosan embedded with ZnO-Fe₃O₄ for Cu (II) removal from aqueous solution. *Int J Biol Macromol* 130:1025–1045. <https://doi.org/10.1016/j.ijbiomac.2019.02.033>
 10. Nebaghe KC, El Boundati Y, Ziat K, Naji A, Rghioui L, Saidi M (2016) Comparison of linear and non-linear method for determination of optimum equilibrium isotherm for adsorption of copper(II) onto treated Martil sand. *Fluid Phase Equilib* 430(Ii):188–194. <https://doi.org/10.1016/j.fluid.2016.10.003>
 11. Khan J, Lin S, Nizeyimana JC, Wu Y, Wang Q, Liu X (2021) “Removal of copper ions from wastewater via adsorption on modified hematite (α -Fe₂O₃) iron oxide coated sand. *J Clean Prod* 319(August):128687. <https://doi.org/10.1016/j.jclepro.2021.128687>
 12. Shahrashoub M, Bakhtiari S (2020) Journal Preof. Microporous Mesoporous Mater 110692. <https://doi.org/10.1016/j.micromeso.2020.110692>
 13. Biswas S, Meikap BC, Sen TK (2019) Adsorptive removal of aqueous phase copper (Cu²⁺) and nickel (Ni²⁺) metal ions by synthesized biochar–biopolymeric hybrid adsorbents and process optimization by response surface methodology (RSM). *Water Air Soil Pollut* 230(8): 2019. <https://doi.org/10.1007/s11270-019-4258-y>.
 14. Bagheri M, Azizian S, Jaleh B, Chehregani A (2014) Journal of industrial and engineering chemistry adsorption of Cu (II) from aqueous solution by micro-structured ZnO thin films. *J Ind Eng Chem* 20(4):2439–2446. <https://doi.org/10.1016/j.jiec.2013.10.024>
 15. Dhiman V, Kondal N (2021) ZnO nanoadsorbents : a potent material for removal of heavy metal ions from wastewater. *Colloid Interface Sci Commun* 41(January): 100380. <https://doi.org/10.1016/j.colcom.2021.100380>
 16. Nalwa K (2017) Synthesis of ZnO nanoparticles and its application in adsorption. *Adv Mater Proc* 2(11):697–703. <https://doi.org/10.5185/amp/2017/696>
 17. Zhang F, Chen X, Wu F, Ji Y (2016) High adsorption capability and selectivity of ZnO nanoparticles for dye removal. *Colloids Surfaces A Physicochem Eng Asp* 509:474–483. <https://doi.org/10.1016/j.colsurfa.2016.09.059>
 18. Nagpal UMK, Bankar AV, Pawar NJ, Kapadnis BP, Zinjarde SS (2011) Equilibrium and kinetic studies on biosorption of heavy metals by leaf powder of paper mulberry (*Broussonetia papyrifera*). *Water Air Soil Pollut* 215(1–4):177–188. <https://doi.org/10.1007/s11270-010-0468-z>
 19. Boon C et al (2018) A review of ZnO nanoparticles as solar photocatalysts : synthesis, mechanisms and applications. *Renew Sustain Energy Rev* 81(August 2017):536–551. <https://doi.org/10.1016/j.rser.2017.08.020>
 20. Kolodziejczak-Radzimska et al (2014) Zinc oxide-from synthesis to application: a review. *Materials (Basel)* 7(4):2833–2881. <https://doi.org/10.3390/ma7042833>
 21. Zno M, Oxide NG (2017) Multifunctional ZnO graphene oxide hybrids nanocomposites for effective water remediation : effective sunlight driven degradation of organic dyes and rapid heavy metal adsorption. *Chem Eng J*. <https://doi.org/10.1016/j.cej.2017.05.105>
 22. Taha A, Da E, Hassanin HA (2021) Modified activated carbon loaded with bio-synthesized Ag / ZnO nanocomposite and its application for the removal of Cr (VI) ions from aqueous solution. *Surf Interfaces* 23(January):e01440. <https://doi.org/10.1016/j.surfin.2021.100928>
 23. Thi A, Pung S, Sreekantan S, Matsuda A (2019) Mechanisms of removal of heavy metal ions by ZnO particles. *Heliyon* (March):e01440. <https://doi.org/10.1016/j.heliyon.2019.e01440>
 24. Alhan S, Nehra M, Dilbaghi N, Kumar N, Kim K, Kumar S (2019) Potential use of ZnO @ activated carbon nanocomposites for the adsorptive removal of Cd²⁺ ions in aqueous solutions. *Environ Res* 173(March):411–418. <https://doi.org/10.1016/j.envres.2019.03.061>
 25. Modwi A, Khezami L, Taha K, Houas A (2017) Fast and high efficiency adsorption of Pb(II) ions by Cu/ZnO composite. *Mater Lett (Ii)*. <https://doi.org/10.1016/j.matlet.2017.02.089>
 26. Prajapati AK, Mondal MK (2021) Novel green strategy for CuO – ZnO – C nanocomposites fabrication using marigold (*Tagetes spp*) flower petals extract with and without CTAB treatment for adsorption of Cr (VI) and Congo red dye. *J Environ Manage* 290(April):112615. <https://doi.org/10.1016/j.jenvman.2021.112615>
 27. Radhakrishnan A, Rejani P, Khan JS, Beena B (2016) Ecotoxicology and environmental safety effect of annealing on the spectral and optical characteristics of nano ZnO : evaluation of adsorption of toxic metal ions from industrial waste water. *Ecotoxicol Environ Saf* 133:457–465. <https://doi.org/10.1016/j.ecoenv.2016.08.001>
 28. Sharma M et al (2020) Solar light assisted degradation of dyes and adsorption of heavy metal ions from water by CuO–ZnO tetrapodal hybrid nanocomposite. *Mater Today Chem* 17:100336. <https://doi.org/10.1016/j.mtchem.2020.100336>
 29. Shukla P, Shukla JK (2018) Facile sol-gel synthesis and enhanced photocatalytic activity of the V₂O₅-ZnO nanoflakes. *J Sci Adv Mater Devices* 3(4):452–455. <https://doi.org/10.1016/j.jsamd.2018.09.005>
 30. Yasoda B, Kumar KS, Ramanadha M, Sudharani A, Vijayalakshmi RP (2020) Enhanced magnetic and optoelectronic properties of Cu-doped ZnO: Mn nanoparticles synthesized by solution combustion technique. *J Supercond Nov Magn* 33(5):1413–1421. <https://doi.org/10.1007/s10948-019-05364-6>
 31. Modwi A, Ghanem MA, Al-Mayouf AM, Houas A (2018) Lowering energy band gap and enhancing photocatalytic properties of Cu/ZnO composite decorated by transition metals. *J Mol Struct* 1173:1–6. <https://doi.org/10.1016/j.molstruc.2018.06.082>
 32. Truong TT, Pham TT, Truong TTT, Pham TD (2021) Synthesis, characterization of novel ZnO/CuO nanoparticles, and the applications in photocatalytic performance for rhodamine B dye degradation. *Environ Sci Pollut Res*. <https://doi.org/10.1007/s11356-021-17106-0>
 33. Asikuzun E, Ozturk O, Arda L, Terzioglu C (2018) Preparation, growth and characterization of nonvacuum Cu-doped ZnO thin films. *J Mol Struct* 1165:1–7. <https://doi.org/10.1016/j.molstruc.2018.03.053>
 34. Wang M et al (2016) Sol-gel-derived ZnO/Cu/ZnO multilayer thin films and their optical and electrical properties. *Mater Sci Semicond Process* 51:55–59. <https://doi.org/10.1016/j.mssp.2016.04.020>
 35. Joshi K, Rawat M, Gautam SK, Singh RG, Ramola RC, Singh F (2016) Band gap widening and narrowing in Cu-doped ZnO thin films. *J Alloys Compd* 680:252–258. <https://doi.org/10.1016/j.jallcom.2016.04.093>
 36. Nimbalkar AR, Patil MG (2017) Synthesis of highly selective and sensitive Cu-doped ZnO thin film sensor for detection of H₂S gas. *Mater Sci Semicond Process* 71(June):332–341. <https://doi.org/10.1016/j.mssp.2017.08.022>
 37. Yousefi HR, Hashemi B (2019) Photocatalytic properties of Ag@ Ag-doped ZnO core-shell nanocomposite. *J Photochem Photobiol A Chem* 375:71–76. <https://doi.org/10.1016/j.jphotochem.2019.02.008>

38. Hsu KC, Fang TH, Hsiao YJ, Li ZJ (2021) Rapid detection of low concentrations of H₂S using CuO-doped ZnO nanofibers. *J Alloys Compd* 852:157014. <https://doi.org/10.1016/j.jallcom.2020.157014>
39. Jevapatarakul D, T-Thienprasert T, Payungporn S, Chavalit T, Khamwut A, T-Thienprasert, NP (2020) Utilization of cratogeomys formosum crude extract for synthesis of ZnO nanosheets: characterization, biological activities and effects on gene expression of nonmelanoma skin cancer cell. *Biomed Pharmacother* 130(May): 110552. <https://doi.org/10.1016/j.biopha.2020.110552>
40. Motazedi R, Rahaiee S, Zare M (2020) Efficient biogenesis of ZnO nanoparticles using extracellular extract of *Saccharomyces cerevisiae*: evaluation of photocatalytic, cytotoxic and other biological activities. *Bioorg Chem* 101(March):103998. <https://doi.org/10.1016/j.bioorg.2020.103998>
41. Azizi S, Shahri MM, Mohamad R (2017) Green synthesis of zinc oxide nanoparticles for enhanced adsorption of lead ions from aqueous solutions: equilibrium, kinetic and thermodynamic studies. *Molecules* 22(6). <https://doi.org/10.1016/j.bioorg.2020.103998>
42. Abdolali A, Guo WS, Ngo HH, Chen SS, Nguyen NC, Tung KL (2014) Typical lignocellulosic wastes and by-products for biosorption process in water and wastewater treatment: a critical review. *Bioresour Technol* 160:57–66. <https://doi.org/10.1016/j.biortech.2013.12.037>
43. Bayrami A, Haghgooeie S, Rahim Poursan S, Mohammadi Arvanag F, Habibi-Yangjeh A (2020) Synergistic antidiabetic activity of ZnO nanoparticles encompassed by *Urtica dioica* extract. *Adv Powder Technol* 31(5):2110–2118. <https://doi.org/10.1016/j.apt.2020.03.004>
44. Shashanka R, Esgin H, Yilmaz VM, Caglar Y (2020) Fabrication and characterization of green synthesized ZnO nanoparticle based dye-sensitized solar cells. *J Sci Adv Mater Devices* 5(2):185–191. <https://doi.org/10.1016/j.jsamd.2020.04.005>
45. George JM, Mathew B (2020) Green-synthesized Cu₂O nanoaggregates incorporated on β -cyclodextrin for catalytic reduction and electrochemical sensing. *J Iran Chem Soc* 17(10):2613–2626. <https://doi.org/10.1007/s13738-020-01954-7>
46. Azizian S, Bagheri M (2014) Enhanced adsorption of Cu²⁺ from aqueous solution by Ag doped nano-structured ZnO. *J Mol Liq* 196:198–203. <https://doi.org/10.1016/j.molliq.2014.03.043>
47. Ghiloufi I, El Ghoul J, Modwi A, El Mir L (2016) Ga-doped ZnO for adsorption of heavy metals from aqueous solution. *Mater Sci Semicond Process* 42(3):102–106. <https://doi.org/10.1016/j.mssp.2015.08.047>
48. Zhang X, Wang Y, Liu Y, Xu J, Han Y, Xu X (2014) Applied surface science preparation, performances of PVDF/ZnO hybrid membranes and their applications in the removal of copper ions. *Appl Surf Sci* 316:333–340. <https://doi.org/10.1016/j.apsusc.2014.08.004>
49. Qi T, Li W, Li H, Ji K, Chen S, Zhang Y (2021) Yttria-doped Cu/ZnO catalyst with excellent performance for CO₂ hydrogenation to methanol. *Mol Catal* 509(April). <https://doi.org/10.1016/j.mcat.2021.111641>
50. Morales-Mendoza JE, Paraguay-Delgado F (2021) Widening UV–Vis absorption band by Cu doped ZnO and ZnO/CuO composite. *Mater Lett* 291:129494. <https://doi.org/10.1016/j.matlet.2021.129494>
51. Valenzuela F et al (2021) Cu(II), Cd(II), Pb(II) and As(V) adsorption from aqueous solutions using magnetic iron-modified calcium silicate hydrate: adsorption kinetic analysis. *J Water Process Eng* 40(January). <https://doi.org/10.1016/j.jwpe.2021.101951>
52. Dhiman N, Sharma N (2019) Removal of pharmaceutical drugs from binary mixtures by use of ZnO nanoparticles: (Competitive adsorption of drugs). *Environ Technol Innov* 15:100392. <https://doi.org/10.1016/j.eti.2019.100392>
53. Raju P, Deivatamil D, Martin Mark JA, Jesuraj JP (2022) Antibacterial and catalytic activity of Cu doped ZnO nanoparticles: structural, optical, and morphological study. *J Iran Chem Soc* 19(3):861–872. <https://doi.org/10.1007/s13738-021-02352-3>
54. Shashanka R (2021) Investigation of optical and thermal properties of CuO and ZnO nanoparticles prepared by *Crocus Sativus* (Saffron) flower extract. *J Iran Chem Soc* 18(2):415–427. <https://doi.org/10.1007/s13738-020-02037-3>
55. Chauhan AK, Kataria N, Garg VK (2020) Green fabrication of ZnO nanoparticles using *Eucalyptus* spp. leaves extract and their application in wastewater remediation. *Chemosphere* 247:125803. <https://doi.org/10.1016/j.chemosphere.2019.125803>
56. Golmohammadi M, Honarmand M, Ghanbari S (2020) A green approach to synthesis of ZnO nanoparticles using jujube fruit extract and their application in photocatalytic degradation of organic dyes. *Spectrochim Acta - Part A Mol Biomol Spectrosc* 229:117961. <https://doi.org/10.1016/j.saa.2019.117961>
57. Ganesh M, Lee SG, Jayaprakash J, Mohankumar M, Jang HT (2019) *Hydnocarpus alpina* Wt extract mediated green synthesis of ZnO nanoparticle and screening of its anti-microbial, free radical scavenging, and photocatalytic activity. *Biocatal. Agric. Biotechnol* 19(March):101129. <https://doi.org/10.1016/j.cbab.2019.101129>
58. Chakraborty S, Farida JJ, Simon R, Kasthuri S, Mary NL (2020) *Averrhoa carambola* fruit extract assisted green synthesis of ZnO nanoparticles for the photodegradation of Congo red dye. *Surf Interfaces* 19(February):1004880. <https://doi.org/10.1016/j.surfin.2020.100488>
59. Nazir H, Salman M, Athar M, Farooq U, Wahab A, Akram M (2019) Citric acid functionalized *Bougainvillea spectabilis*: a novel, sustainable, and cost-effective biosorbent for removal of heavy metal (Pb²⁺) from waste water. *Water Air Soil Pollut* 230(12). <https://doi.org/10.1007/s11270-019-4360-1>
60. Piccin JS, Dotto GL, Pinto LAA (2011) Adsorption isotherms and thermochemical data of FDandC RED N° 40 Binding by chitosan. *Brazilian J Chem Eng* 28(2):295–304. <https://doi.org/10.1590/S0104-66322011000200014>
61. Hasan M, Ahmad AL, Hameed BH (2008) Adsorption of reactive dye onto cross-linked chitosan/oil palm ash composite beads. *Chem Eng J* 136(2–3):164–172. <https://doi.org/10.1016/j.cej.2007.03.038>

Publisher's Note Springer Nature remains neutral with regard to jurisdictional claims in published maps and institutional affiliations.

Springer Nature or its licensor holds exclusive rights to this article under a publishing agreement with the author(s) or other rightsholder(s); author self-archiving of the accepted manuscript version of this article is solely governed by the terms of such publishing agreement and applicable law.